J Solid State Electrochem (2005) 9: 665–673
DOI 10.1007/s10008-004-0637-3

ORIGINAL PAPER

Adriane V. Rosario · Ernesto C. Pereira

Influence of the crystallinity on the Li^+ intercalation process in Nb_2O_5 films

Received: 27 August 2004 / Revised: 4 October 2004 / Accepted: 19 November 2004 / Published online: 10 June 2005

Abstract Nb_2O_5 thin films were prepared by the Pechini method. The effect of the film crystallinity on the electrochemical and electrochromic properties was investigated. A relationship between the crystalline structure and the Li^+ intercalation/extraction process, stability and kinetics was observed. A significant decrease in the electrochemical response was observed as a function of the number of cycles for films treated at 400 and 450 °C. However, as the calcination temperature increases this effect disappears. XRD studies shown that at 400 °C, the material is amorphous, evolving to orthorhombic phase. The transmittance variation as well as the coloration efficiency increases as the temperature is increased. In the initial cycles the intercalation charge is higher for the amorphous oxide than for the orthorhombic phase. However, the variation in the optical density is small. On the other hand, the charge of the orthorhombic phase oxide does not change. These results suggest that there are two different processes associated with Li^+ intercalation, but only one of them leads to the coloration process.

Keywords Nb_2O_5 · Electrochromism · Li^+ intercalation · Pechini method

Introduction

Niobium pentoxide presents cathodic electrochromism, in a similar way to WO_3, which is described by the following equation [1]:

A. V. Rosario · E. C. Pereira (✉)
Laboratório Interdisciplinar de Eletroquímica e Cerâmica,
Centro para o Desenvolvimento de Materiais Cerâmicos,
Departamento de Química, Universidade Federal de São Carlos,
CP: 676, 13560-970 São Carlos, Brazil
E-mail: decp@power.ufscar.br
Tel.: +55-16-2608214
Fax: +55-16-2615215

$$\underset{\text{(Transparent)}}{Nb_2O_5} + xA^+ + xe^- \rightleftharpoons \underset{\text{(Blue)}}{A_xNb_2O_5}, \quad (1)$$

where $A = H^+$ or Li^+.

Nb_2O_5 has a complex crystalline structure, with 12 identified structural isomers. The most common phases are denominated T—orthorhombic, TT—pseudohexagonal, M—tetragonal and H—monoclinic [2]. The formation of these structures is not only dependent on the preparation temperature and time, but also on other factors (e.g. starting material, heating rate and impurity content). The T-phase consists of an orthorhombic unit cell, with each Nb atom surrounded by six or seven oxygen atoms, thus forming distorted octahedral or pentagonal bipyramid co-ordination structures, respectively [3, 4]. According to Ikeya et al. [4], the hexagonal unit cell of the TT-phase contains only half of the equivalent formula ($NbO_{2.5}$), with a one oxygen deficiency per unit cell. The polyhedra are distorted by the oxygen deficiency. In the three-dimensional structure, each Nb atom is surrounded by six, seven or eight oxygen atoms, producing tetragonal, pentagonal or hexagonal bipyramid unit cells. The H-Nb_2O_5 phase is monoclinic and the M-Nb_2O_5 phase is tetragonal, with the latter phase considered to be a two-dimensionally ordered variant of former. Both phases consist of Nb atoms with octahedral co-ordination [5].

When Li^+ ions are inserted in the Nb_2O_5 structure, its films display electrochromic properties, with fast and reversible coloration. However, a strong dependence of the electrochromic properties on the preparation method and treatment temperature has been observed. Fu et al. [6], obtained films with a transmittance variation of 25% and coloration efficiency between 8 cm^2/C and 21 cm^2/C. A simple thermal treatment at 550 °C, leads to a coloration efficiency of 40 cm^2/C. Yoshimura et al. [7], also observed the effect of temperature on the electrochromic properties of Nb_2O_5 films produced by sputtering. The best results were observed for the samples obtained with the substrate heated at 500 °C. In this case, the transmittance variation was of 45% and

remained stable for 1,000 intercalation/deintercalation cycles. Schmitt and Aegerter [8], studied not only the effect of temperature, but also that of dopant addition in films prepared by the sol–gel method. According to the authors, the amorphous films display brown coloration during the intercalation process, while the samples treated at higher temperatures presented blue coloration. The coloration efficiency varied between 16 cm^2/C and 28 cm^2/C. A coloration efficiency of 38 cm^2/C in formic acid solution, was obtained by Ohtani et al. [9], for the films prepared using the sol–gel route at 460 °C. This value is relatively high for an amorphous film compared to the studies discussed above. However, it is important to stress that proton mobility is superior to that of Li^+.

Although several studies have detailed the effect of structure on the properties of the material, the understanding of the coloration mechanism is still not completely understood. Thus, this paper intends to contribute to the understanding of the mechanism involved in the Nb_2O_5 coloration process.

The aim of this work was to study the evolution of structural properties during heat treatment and the consequences on the optical and electrochemical behavior. In this sense, Nb_2O_5 films were prepared using the Pechini method [10], calcinated at different temperatures and characterized by SEM, XRD and electro-optical measurements.

Experimental

To prepare the niobium precursor resin, citric acid (CA—p.a., Synth) was added to ethylene glycol (EG—p.a., Merck) under stirring at 70 °C. After the dissolution of citric acid, the niobium salt, $NH_4H_2[NbO(C_2O_4)_3]3H_2O$ (CBMM—Brazil) was added slowly under stirring. The solution was prepared using an Nb:CA:EG molar ratio of 1:10:40. Films were prepared by dip coating of the resin on ITO coated glass (Donnelly, 20 Ω), at a withdrawal speed of 2.0 cm/min. The samples were treated at 110 °C for 60 min to promote the polymerization reaction between CA and EG and then calcinated for 120 min at temperatures between 400 °C and 650 °C. The powder samples were prepared under the same conditions and then pulverized to eliminate agglomerates.

Cyclic voltammetry and chronoamperometry measurements were performed using a PARC EG&G mode 263 potenciostat/galvanostat. Measurements were performed in a three-electrode cell. As a counter electrode and quasi reference electrode a Pt plate and a silver wire were used. The Nb_2O_5 films deposited on ITO glass were used as working electrodes. The measurements were performed at room temperature in 0.1 mol/L $LiClO_4$ (p.a. Aldrich) in acetonitrile (p.a. Merck). A flat window electrochemical cell was used in the electro-optical measurements. The transmittance spectra were obtained using an UV–Vis–NIR spectrophotometer (Cary model 5G). The structure of oxide films was analyzed by X-ray diffraction with a diffractometer (Siemens model D5000), using CuKα radiation (λ = 1.54 Å). The surface morphology was analyzed by Scanning electron microscopy (SEM—Zeiss model 940A). The thickness of the deposited films is measured by SEM to be between 100 nm and 200 nm.

Results and discussion

Structural and morphological characterization

Figure 1a presents the effect of temperature on the crystallization process of Nb_2O_5 powders. It can be observed that, for the powder prepared at 400 °C, the material is completely amorphous. At 450 °C it is possible to identify the beginning of the crystallization process and for temperatures above 500 °C a crystalline material can be observed. From 500 °C is observed the peak separation attributed to the (180) and (200) and

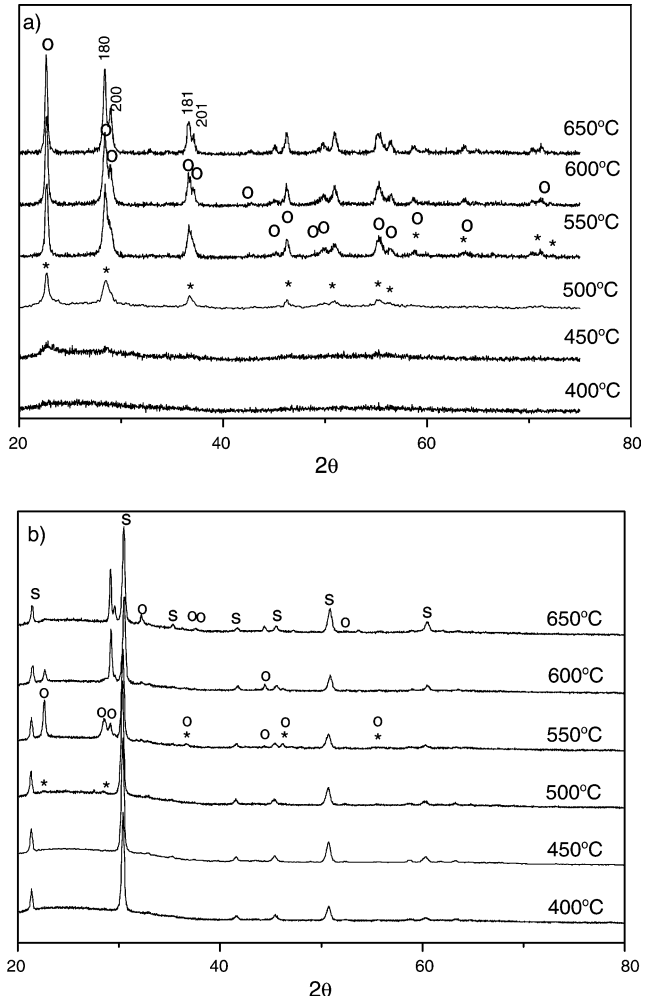

Fig. 1 XRD patterns of Nb_2O_5 in form of **a** powders and **b** films calcined between 400 and 650°. *s* substrate (ITO), *o* orthorhombic phase and * hexagonal phase

(181) and (201) planes that differentiate the orthorhombic phase (T-Nb_2O_5) [11] of the pseudohexagonal phase (TT-Nb_2O_5) [12]. The films present the same crystallization process evolution (Fig. 1 b), however, the films treated at 600 and 650 °C present a displacement of the peaks related to the (180) and (200) planes, as well as a peak intensity decrease for the (001) plane ($2\theta = 22.61$). This fact can be explained in terms of the growth-oriented effect produced by the substrate. The possibility of the presence of the pseudohexagonal phase at lower temperatures should not be discarded, though its existence is not evident in a first analysis. Calculation of the lattice parameters and the unit cell volume suggest the existence pseudohexagonal phase at 500 °C. A very expressive deviation of the lattice parameters comparing to the theory values of the orthorhombic phase [11] were observed for films prepared at 550 and 600 °C, leads to an indication of a secondary phase present. In this case, we think that the substrate contributed to the stabilization of the TT-phase. There is controversy, about the existence of the pseudohexagonal phase, once the literature described the TT-phase as a metastable form that occur as a disordered orthorhombic phase [4, 5, 13]. According to Weismann et al. [13], the TT-phase is stabilized by impurities such as OH^-, Cl^-, or oxygen vacancies. Narendar and Messing [5] synthesized Nb_2O_5 from peroxo-citrato-niobium precursor and shown that the TT-Nb_2O_5 is the first crystalline phase observed after de precursor decomposition above 580 °C. TT → T phase transition occur around 800 °C.

It is important to point out that the majority of the Nb_2O_5 films described in the literature are in the hexagonal phase. Barros Filho et al. [14], for example, prepared films by the conventional alkoxides sol–gel method and observed that the orthorhombic phase is only observed at 800 °C. The ease of obtaining different phases at lower temperatures than those necessary for other preparation methods is one of the advantages of the Pechini method.

The average crystallite sizes, calculated using the Scherrer method, are presented in Table 1. The results show an increase in the crystallite size as a function of the calcination temperature. This behavior is expected, as mass transport is more effective at higher temperatures.

If we considering that the crystalline growth kinetic follows the empirical equation [15]:

$$D^n - D_o^n = kt, \tag{2}$$

where, D is the crystallite size, D_o is the initial nuclei size, k is a constant that depends of the temperature (T), t is the time and n the growth kinetic exponent.

For a process thermally activated and if $D \gg ; D_o$, it is possible then to expresses the Eq.1 as a form of the Arrhenius equation:

$$D^n = k_0 \exp\left(\frac{-E}{RT}\right) t, \tag{3}$$

where k_o is the constant independent of T, R is gas constant, T is absolute temperature, and E is activation energy to mass transport process.

Figure 2 shows the plot of lnD in function of the $1/T$. Powder samples show linear behavior while film samples present change in the slope of curve. The non-linearity suggests changes in the mass transport mechanism that could be one more indicative of the presence of the pseudohexagonal phase. This behavior could be an effect produced by an oriented growth due the substrate.

Figure 3 shows the evolution of the film surface morphology as the calcination temperature is increased. For samples treated at the lower temperatures, the presence of an anomalous growth form is observed, which decreases as the temperature is increased. It is possible that these structures can be related to the presence of polyester residues, as, in the previously published thermal analysis studies [16], it was observed that the crystallization process occurs simultaneously with the end of the decomposition of the organic precursor. For temperatures above 550 °C these anomalous forms are not observed. Above this temperature the films display isotropic morphology with well-defined particles.

Electrochemical and electrochromic characterization

The analysis of the electrochemical results shows the effect of crystallization on the oxide properties. Figure 4 shows the cyclic volammograms of samples prepared at different temperatures. The first important piece of information to be obtained from Fig. 4 regards the effect of the cycling on the cathodic and anodic current response. Films treated at 400 °C present a decrease in the current density as a function of the number of cycles. This effect is also quite accentuated for the sample prepared at 450 °C. However, as the calcination temperature increases, this effect practically disappears. Table 2 shows the electrochemical parameters obtained from the voltammetric curves. An increase is observed in the cathodic current and cathodic charge densities (i_c and Q_c) as well as in the anodic current and anodic charge densities (i_a and Q_a) up to a temperature of 500 °C.

Table 1 Average crystallite size for the (180) plane

Nb_2O_5	Crystallite size (Å)					
	400 °C	450 °C	500 °C	550 °C	600 °C	650 °C
Powder	—	—	84	103	169	252
Film	—	—	152	176	524	647

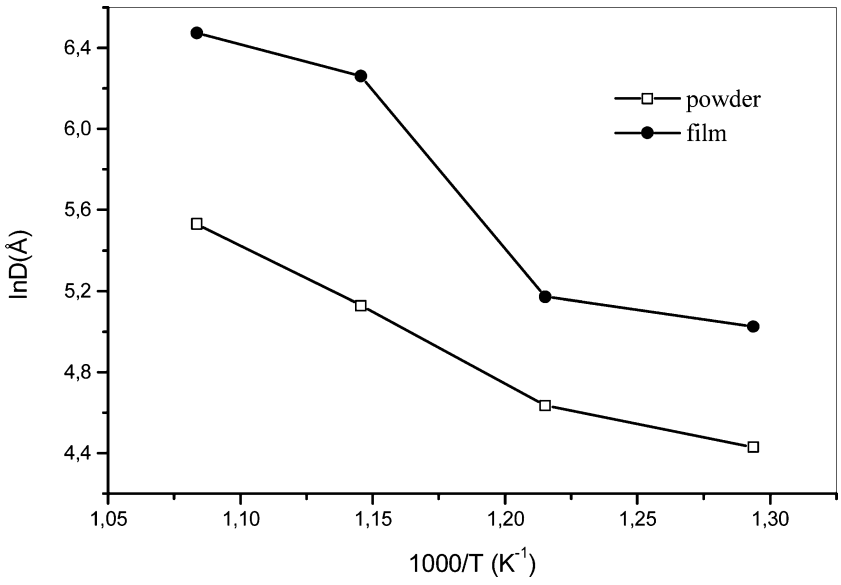

Fig. 2 Dependence of the crystallite size with the temperature

Above 550 °C the observed values decrease. The sample treated at 650 °C presents the lowest values, even lower than the sample treated at 400 °C.

Another important point concerns to the reversibility of the redox process. The anodic peak potential (E_{pa}) becomes more negative as the thermal treatment temperature increases. For the films treated at lower temperatures the potential also decreases with cycling, while for the films treated at temperatures between 550 °C and 650 °C it remains constant. Moreover, it is also observed that the Q_a/Q_c ratio decreases with cycling for the films treated at temperatures between 400 °C and 550 °C. In contrast, for the films calcinated at 600 and 650 °C, the value of Q_a/Q_c increases as the number of cycles increases (Fig. 5). This last observation indicates that the reduction process and Li^+ intercalation process is favored by the oxide structure, and not by the surface area. This is because the surface area of an oxide decreases as the thermal treatment temperature increases, as a consequence of the grain growth process. In principle, it is expected that an amorphous material would present a more open structure, which facilitates the intercalation process. This premise is true in the case of the WO_3 films. As demonstrated in the literature [17, 18], the crystalline WO_3 films present an electrochromic performance inferior to that of the amorphous film. On the other hand, the present results show that amorphous Nb_2O_5 films, in the first cycles, present a relatively high charge response, which decreases in the subsequent cycles. This effect decreases for the films prepared at higher temperatures. Bueno et al. [19] demonstrated that the addition of small amounts of $LiCF_3SO_3$ during the synthesis of the Nb_2O_5 films prepared by the alkoxide method improves their electrochemical properties. The authors verified an increase in the electrochemical reversibility of the oxide and attributed this effect to a more open crystalline arrangement, which was due to presence of Li atoms in the structure. Thus, the insertion of a larger amount of Li^+ during the electroreduction of the film would be facilitated. On the other hand, the results presented in Fig. 4 permit the proposal of a different hypothesis: The amorphous material uses part of the Li^+ inserted in the initial cycles to stabilize its structure, while maintaining them in the lattice. This proposition is discussed in the following section.

The samples were submitted to 500 sequential potential steps, between 0.5 V and −1.5 V over a period of 100 s and the transmittance response as a function of time is shown in Fig. 6. The transmittance variation (ΔT) increases as the calcination temperature increases up to 600 °C. For 650 °C, the ΔT% values decrease (Fig. 6). For all the temperatures, an accentuated loss of transmittance variation is observed in the first 30 cycles, and this loss is still higher for films treated between 400 °C and 550 °C.

As can be observed in Fig. 7, although the samples treated at 550 and 600 °C have higher ΔT % values, the sample treated at 650 °C presented a reasonably high transmittance variation ($\Delta T \cong 45\%$) and moreover, displayed good stability. For the samples calcinated at 400, 550 and 600 °C the film transmittance in the bleached state (T_b) also decreases during the cycling. However, for the last two temperatures, the transmittance in the colored state (T_c) is constant. For the films prepared at 400 °C, it is observed that the T_c transmittance also decreases. This behavior should lead to an electrochromic activity loss, even for a small number of cycles.

The fact that the amorphous samples present the smallest ΔT values could be attributed to the effect of light scattering caused by structural defects. However, this mechanism is not possible, as these samples presented transmittance values in the bleached state as high

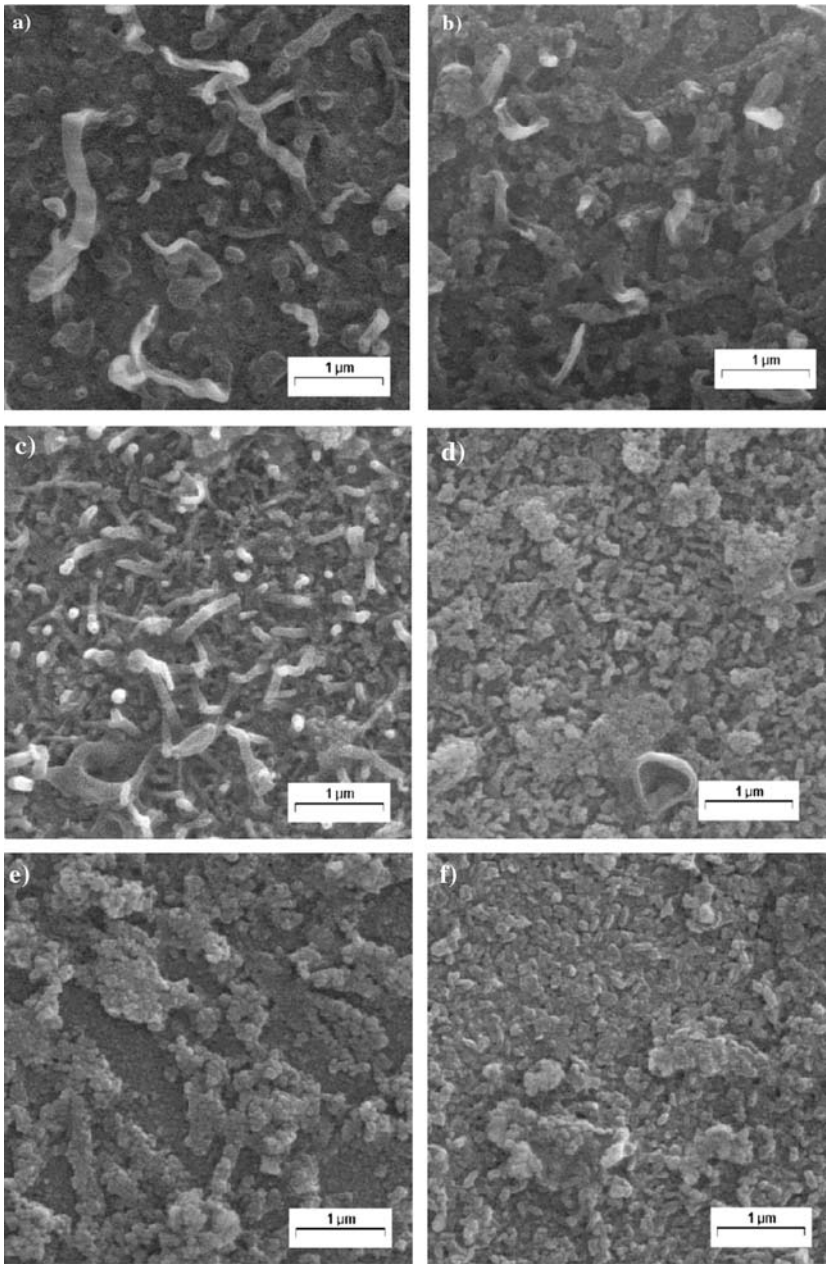

Fig. 3 Micrographs of Nb_2O_5 surface films: **a** 400 °C, **b** 450 °C, **c** 500 °C, **d** 550 °C, **e** 600 °C, **f** 650 °C. Magnification ×20,000

as those obtained for the crystalline films. Therefore, this characteristic could be associated with the fact that the films treated at low temperatures remained colored after the reduction–oxidation process, indicating that a part of Li^+ ions remain in the oxide lattice. For this reason, the decrease in the maximum transmittance value (bleached state) is observed as the number of cycles increases.

XRD results presented in Fig. 1 demonstrated that at 400 and 450 °C the oxide is amorphous, it evolves to the T-Nb_2O_5 phase with an orthorhombic structure. Therefore, unlike WO_3, the higher the crystallinity of Nb_2O_5, the higher is its optical variation (and stability of this property). Yoshimura et al. [20] also verified that Nb_2O_5 films present an increase in the optical variation as the crystallinity increases. This effect was observed for Nb_2O_5 films formed by magnetron sputtering, where the films prepared using a substrate heated to 500 °C present high crystallinity (hexagonal phase), while the sample prepared with an unheated substrate was totally amorphous.

The ratio of the optical variation with the insertion charge is shown in Table 3. Coloration efficiency, CE, tends to increase as the temperature increases. The coloration efficiency also increases after the first cycle. Although the samples treated at 650 and 600 °C presented the smallest intercalation charge during the voltammetric measurement, it is observed that these samples have high CE values (50–65 cm^2C^{-1} and 40–50 cm^2C^{-1} for the samples treated at 650 and 600 °C, respectively).

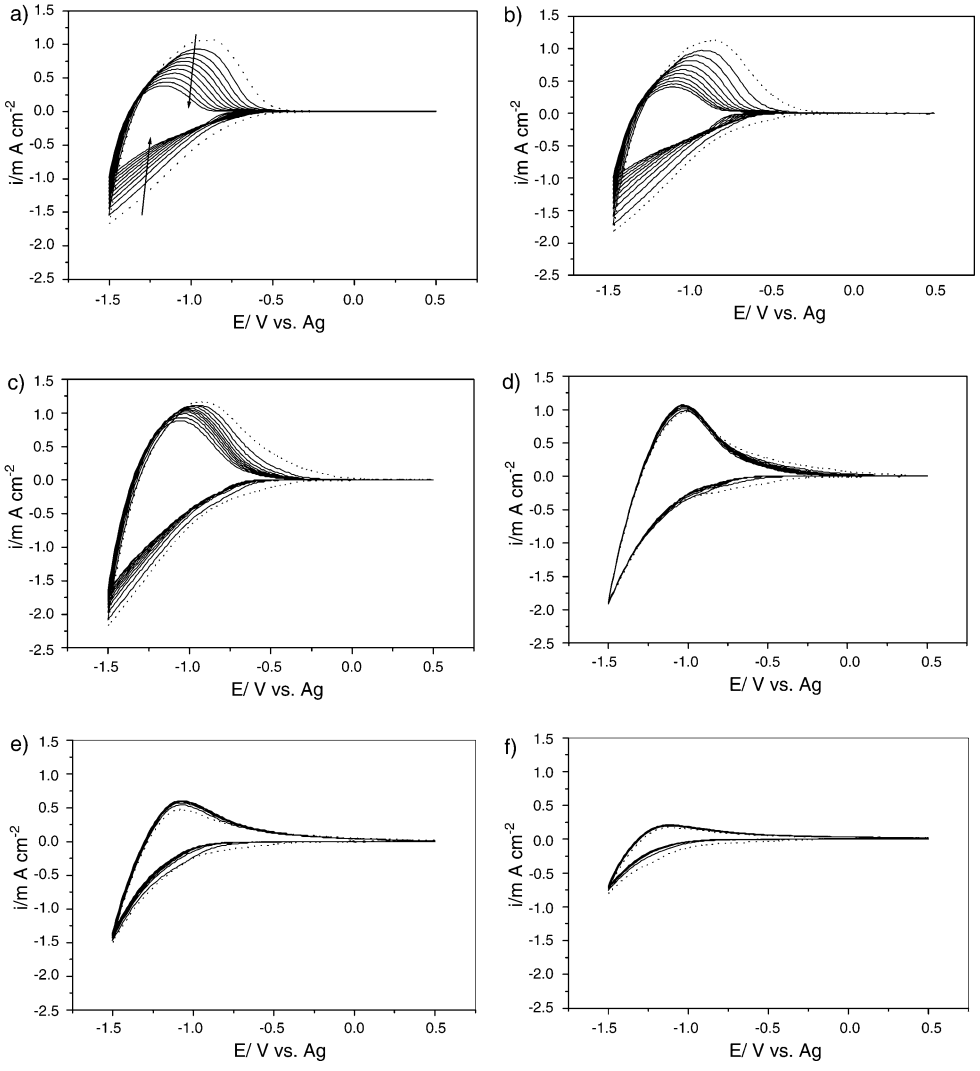

Fig. 4 Cyclic voltammograms of Nb_2O_5 films treated at: **a** 400 °C, **b** 450 °C, **c** 500 °C, **d** 550 °C, **e** 600 °C, **f** 650 °C, $v = 50$ mV/s , $T = 25$ °C. (.....) first cycle and (————-) ten following cycles

Table 2 Charge densities, cathodic and anodic charge ratio and anodic peak potential for 1st and 10th cycles

T(°C)	Q_c(mC cm^{-2})	Q_a(mC cm^{-2})	Q_a/Q_c(%)	E_{pa}(V)
400				
1st cycle	−16.03	11.71	73.1	−0.88
10th cycle	−7.89	2.96	32.5	−1.15
450				
1st cycle	−18.43	13.37	72.50	−0.89
10th cycle	−9.27	3.90	42.09	−1.14
500				
1st cycle	−21.21	14.82	69.9	−0.93
10th cycle	−13.63	8.72	64.01	−1.07
550				
1st cycle	−15.19	11.36	74.8	−1.01
10th cycle	−13.55	9.93	73.25	−1.02
600				
1st cycle	−11.62	5.76	49.6	−1.08
10th cycle	−8.32	6.88	82.64	−1.06
650				
1st cycle	−6.03	2.41	40.0	−1.11
10th cycle	−3.63	2.91	80.3	−1.13

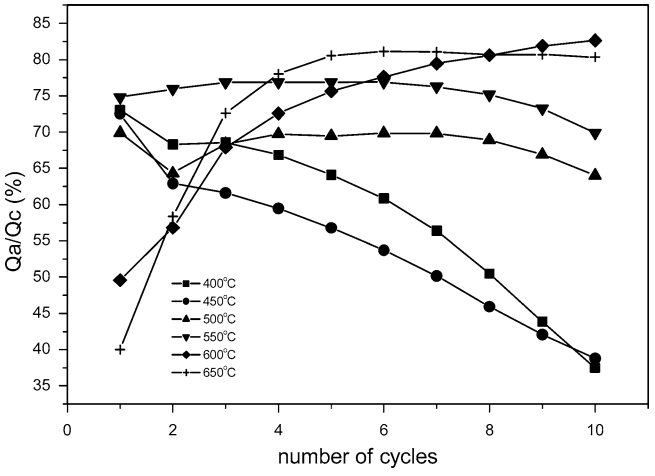

Fig. 5 Anodic and cathodic charges ratio in function of cycling

These results provide more evidence that not all the Li^+ intercalated in the oxide structure contributes to the coloration.

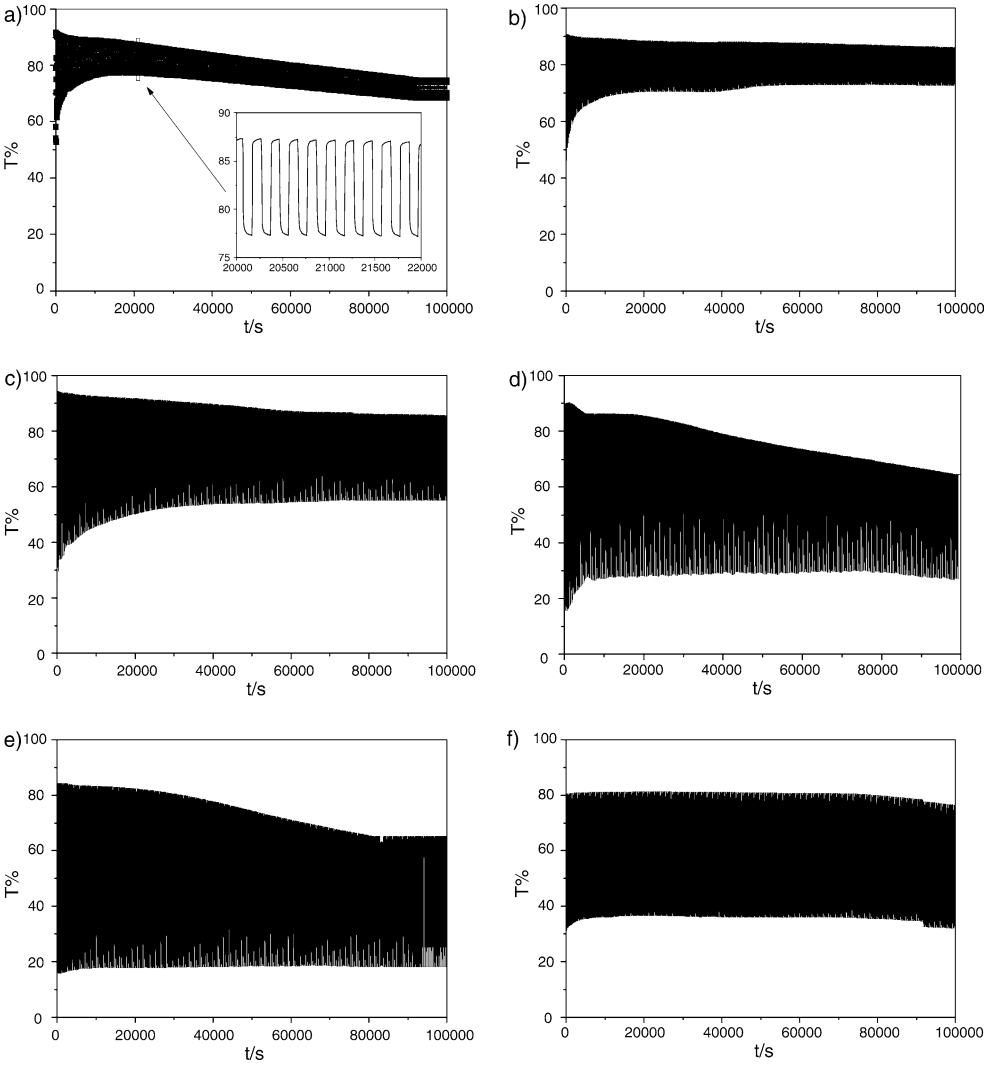

Fig. 6 Optical transmittance to consecutive chronoamperometric steps (0.5 V/100 s to −1.5 V/100 s). **a** 400 °C, **b** 450 °C, **c** 500 °C, **d**550 °C, **e** 600 °C, **f** 650 °C

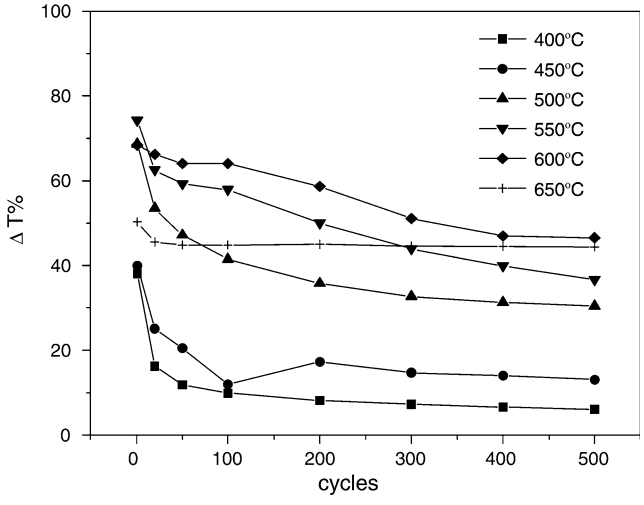

Fig. 7 Transmittance variation profile in function of the cycles number

In order to compare the electro-optical response of the films, the chronoamperometric charge and the optical density (OD) curves were normalized in function of their maximum values (OD = −log *T*). The normalized curves for the films treated at 600 °C are presented in Fig. 8. The 10th and 500th Li^+ intercalation (a,c) and extraction (b,d) cycles are shown. The first observation concerning the difference between the reduction/coloration and oxidation/bleaching process is that the kinetics of the coloration process are slower than the kinetics of the bleaching process. For the first cycles it was observed that, in the insertion process, the charge curves and

Table 3 Coloration efficiency values, CE (cm^2/C), at different cycling times

Cycle	400 °C	450 °C	500 °C	550 °C	600 °C	650 °C
1	4.4	14.2	13.5	14.5	23.9	40.1
20	9.4	16.2	25.2	17.5	48.6	50.7
50	7.6	16.4	22.6	17.6	47.7	57.9
100	7.5	16.4	23.0	18.0	50.9	50.0
200	8.3	17.5	20.2	16.9	43.1	59.0
300	8.1	17.3	20.0	17.2	44.7	63.8
400	8.7	16.5	20.4	17.4	40.2	54.9
500	8.8	16.5	21.0	17.4	40.7	65.9

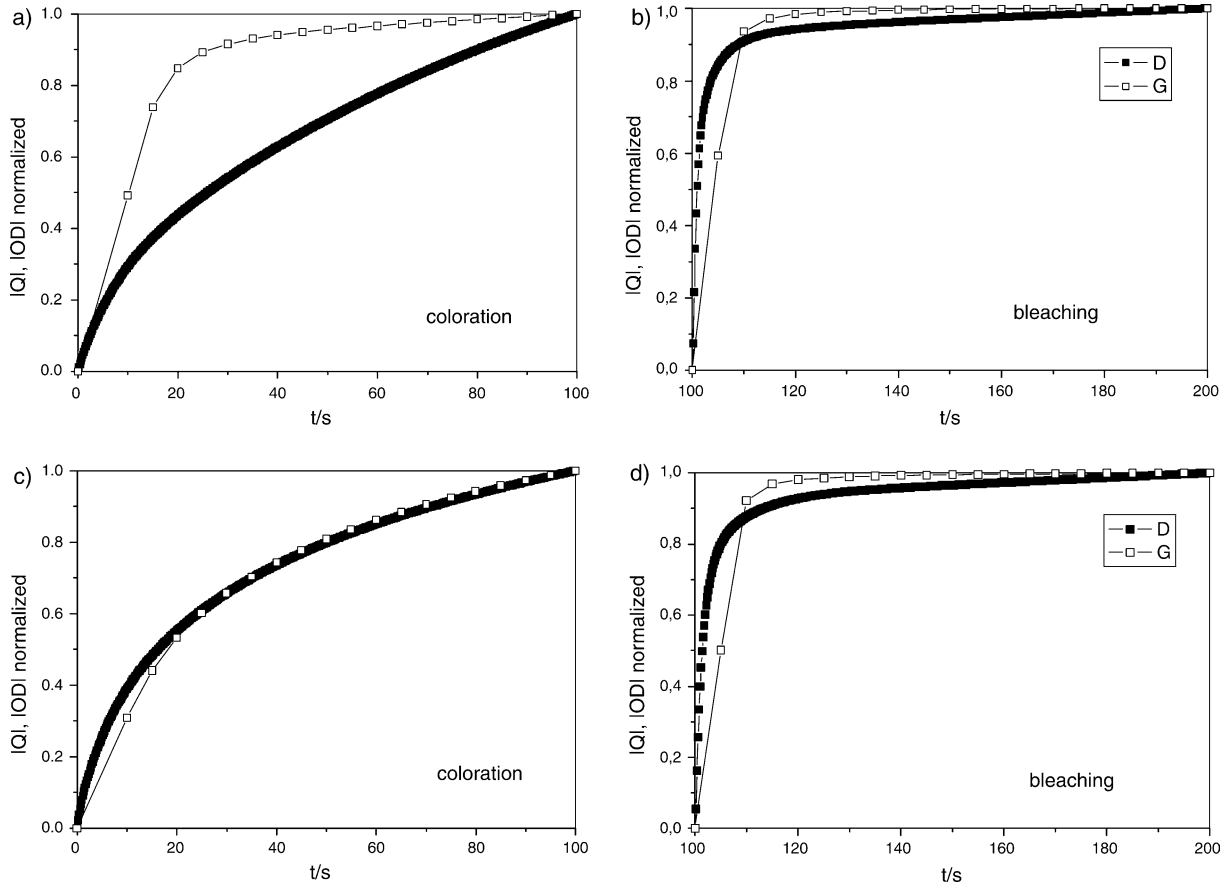

Fig. 8 Charge density and optical density in function of the polarization time to films treated at 600 °C in different cycling times. Charge density (*filled square*) and optical density (*open square*), **a** 10th coloration cycle **b** 10th bleaching cycle, **c** 500th coloration cycle and **d** 500th bleaching cycle

optical density are quite distinct. During the reduction, the electrochemical process is slower than the coloration process of the film, once the film achieves its coloration limit at the beginning of the electro-reduction process. On the other hand, during anodic polarization of the film, it is observed that the electrochemical process is faster at shorter times, but for longer times the bleaching occurs before the whole charge is extracted. However, this difference decreases with further film cycling. The synchrony between the optical and charge curves is achieved by 50th cycle. On the other hand, for films prepared at 400 °C the difference between the charge and the optical curves is maintained up to the 500th cycle. The samples treated between 450 °C and 550 °C also displayed differences between the electrochemical and optical processes, however, it was observed that this difference decreases with further cycling and also as the temperature increases. Although a profound discussion of these results is quite difficult, it is clear that not all the intercalated Li^+ is involved in the coloration of the film. This fact can be explained because, in spite of the great difference in Q_a/Q_c for all the films, the reversibility of the electrochromic process is maintained upon cycling.

Conclusions

All the parameters involved in the kinetics of the oxide electrocoloration process such as reversibility, Q, ΔT %, CE and life time are highly dependent on the treatment temperature and are mainly related to structural properties of the oxide. The increase in the reversibility of the electrochromic process with increasing treatment temperature indicates that part of the initially inserted Li^+ is maintained in the oxide lattice to stabilize its structure. Everything indicates that the orthorhombic structure (higher temperature) favors the insertion and coloration process of the coloration sites in the oxide. The difference between the optical variation and charge variation curves indicates the possible existence of a secondary process during the intercalation process.

Acknowledgements The authors wish to thank the Brazilian Research Funding Institutions CNPq and FAPESP for their financial support.

References

1. Reichman B, Bard A (1980) J Electrochem Soc 127:241
2. Aegerter MA (2001) Sol Ernergy Mater Sol Cells 68:401
3. Kato VK, Tamura S (1975) Acta Cryst B31:673
4. Ikeya T, Senna M (1988) J Non-Cryst Solids 105:243
5. Narendar V, Messing GL (1997) Chem Mater 9:580

6. Fu Z-W, Kong J-J, Qin Q-Z (1999) J Electrochem Soc 146:3914
7. Yoshimura K, Miki T, Tanemura S (1997) J Electrochem Soc 144:2982
8. Schmitt M, Aegerter MA (2001) Electrochim Acta 46:2105
9. Ohtani B, Iwai K, Nishimoto S-I, Inui T (1994) J Electrochem Soc 141:2439
10. Pechini M P USA patent no. 3.330.697 July 1967
11. JCPDS- 30–873
12. JCPDS- 7–61
13. Ko EI, Weismann JG (1990) Catal Today 8:27
14. Filho DAB, Franco DW, Filho PPA, Alves OL (1998) J Mater Sci 33:2607
15. Aust KT, Palumbo G (1996) Mater Sci Forum 204:44
16. Rosario AV, Pereira EC, J Sol-gel Sci Technol (submited)
17. Kaneko H, Nagao F, Miyake K (1988) J Appl Phys 63:510
18. Wang Z, Hu X (2001) Electrochim Acta 46:1951
19. Bueno PR, Avellaneda CO, Faria RC, Bulhões LOS (2001) Electrochim Acta 46:2113
20. Yoshimura K, Miki T, Iwama S, Tanemura S (1996) Thin Solid Films 235:281–282